



Universiteit  
Leiden  
The Netherlands

## Copper complexes for bioinspired electrocatalysis relevant to the reduction of oxygen

Langevelde, P.H. van

### Citation

Langevelde, P. H. van. (2025, April 16). *Copper complexes for bioinspired electrocatalysis relevant to the reduction of oxygen*. Retrieved from <https://hdl.handle.net/1887/4212226>

Version: Publisher's Version

License: [Licence agreement concerning inclusion of doctoral thesis in the Institutional Repository of the University of Leiden](#)

Downloaded from: <https://hdl.handle.net/1887/4212226>

**Note:** To cite this publication please use the final published version (if applicable).

## Chapter 4

# Mechanistic Investigations into the Selective Reduction of Oxygen by a MCO T3 Site-inspired Dicopper Complex

Understanding how multicopper oxidases (MCOs) reduce oxygen in the trinuclear copper cluster (TNC) is of great importance for development of catalysts for the oxygen reduction reaction (ORR). In this chapter a mechanistic investigation into the ORR activity of the dinuclear copper complex  $[\text{Cu}_2\text{L}(\mu\text{-OH})]^{3+}$  (L=2,7-bis[bis(2-pyridylmethyl)aminomethyl]-1,8-naphthyridine) is reported. This complex is inspired by the dinuclear T3 site found in the MCO active site and confines the Cu centers in a rigid scaffold. We show that the electrochemical reduction of  $[\text{Cu}_2\text{L}(\mu\text{-OH})]^{3+}$  follows a proton-coupled electron transfer pathway and requires a larger overpotential due to the presence of the Cu-OH-Cu motif. In addition, we provide evidence that metal-metal cooperativity takes place during catalysis that is facilitated by the constraints of the rigid ligand framework, by identification of key intermediates along the catalytic cycle of  $[\text{Cu}_2\text{L}(\mu\text{-OH})]^{3+}$ . Electrochemical studies show that the mechanisms of the ORR and hydrogen peroxide reduction reaction (HPRR) found for  $[\text{Cu}_2\text{L}(\mu\text{-OH})]^{3+}$  differ from the ones found for analogous mononuclear copper catalysts. In addition, the metal-metal cooperativity results in an improved selectivity for the four-electron ORR of more than 70%, because reaction intermediates can be stabilized better between both copper centers. Overall, the mechanism of the  $[\text{Cu}_2\text{L}(\mu\text{-OH})]^{3+}$ -catalyzed ORR in this work contributes to understanding of how the cooperative function of multiple metals in close proximity can affect ORR activity and selectivity.

## 4.1 Introduction

The four-electron reduction of oxygen to water plays a key role in fuel cell technology.<sup>1, 2</sup> Currently, the most efficient catalysts for the oxygen reduction reaction (ORR) are Pt-based, which drives up the costs of fuel cell devices and limits their commercial viability.<sup>3-5</sup> Nature has found an efficient way to reduce oxygen in multicopper oxidases (MCOs) using earth-abundant copper.<sup>6</sup> The thermodynamic and kinetic properties of the ORR catalyzed by the MCO enzyme laccase have been compared to those of Pt electrodes.<sup>7-9</sup> Interestingly, immobilization of laccase on electrodes resulted in the selective four-electron reduction of oxygen to water at a lower overpotential than Pt.<sup>7</sup> From this it is apparent that MCOs, especially laccases, are excellent ORR catalysts. Hence, studying catalysts that are inspired by the MCO active site can point scientists towards new design principles for the next generation ORR catalysts.

MCOs are a class of enzymes that couple the oxidation of a variety of substrates to the reduction of oxygen.<sup>6</sup> The MCO active site consists of a mononuclear T1 copper site and the trinuclear copper cluster (TNC) containing the bimetallic T3 and mononuclear T2 sites (**Figure 4.1a**).<sup>10</sup> The T1 site is responsible for the oxidation of substrates and the transfer of electrons to the TNC, where in turn oxygen can bind and is reduced. A combination of spectroscopic and crystallographic studies, supported by computational studies in more recent years, have contributed to the identification of the key intermediates in the catalytic cycle.<sup>11, 12</sup> In addition, an overall mechanism for the four-electron reduction of oxygen was formulated involving these intermediates shown in **Figure 4.2**.<sup>11-14</sup>

The O<sub>2</sub> reduction mechanism to H<sub>2</sub>O comprises of two distinct two-electron transfers. The first two electrons are transferred when dioxygen binds to the fully reduced (FR) state. In studies using MCOs without T1 sites or with T1 sites replaced by Hg<sup>2+</sup>, the peroxide intermediate (PI), formed after this initial electron transfer, could be detected.<sup>15-17</sup> In MCOs with an intact T1 site, the PI cannot be isolated since a rapid, second two-electron transfer will lead to cleavage of the O-O bond and the formation of the native intermediate (NI) state.<sup>17</sup> To complete the catalytic cycle, the NI is re-reduced to the FR state in a process involving 4 protons and 3 electrons.<sup>18</sup> Outside of this catalytic cycle lies the enzyme's resting oxidized (RO) state, to which the NI will slowly decay in the absence of reducing equivalents.<sup>19, 20</sup> Apparent from this mechanism is that in all catalytic intermediates, except the FR, oxygen-derived species bound between multiple copper centers play a key role. The fact that metal-metal cooperativity plays an essential role throughout the MCO mechanism, inspired us to investigate how the ORR activity and selectivity are established at a dinuclear copper site that is inspired by the MCO T3 site.

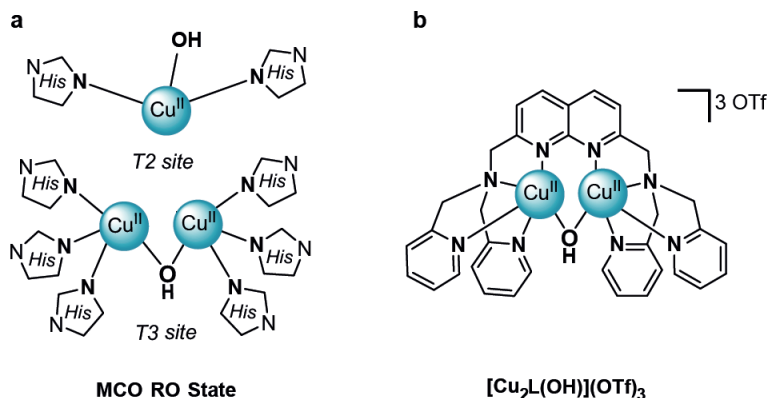


**Figure 4.1** Schematic overview of a) the MCO active site in the RO state with histidines simplified for clarity, and b) structure of the  $[\text{Cu}_2\text{L}(\mu\text{-OH})](\text{OTf})_3$  complex.

The MCO active site has inspired the design of many molecular copper complexes to date, typically supported by polynucleating ligands that feature multiple N-donor atoms that mimic the histidine ligands in the TNC.<sup>21, 22</sup> The coordination chemistry and the reactivity of Cu(I) complexes with oxygen has also been extensively studied.<sup>21-23</sup> In addition, trinuclear copper complexes have been developed to study the role of proton-coupled electron transfers in MCOs.<sup>24</sup> However, when it comes to the ORR reactivity, only a few complexes with multiple metal centers have been investigated to date. Moreover, the catalytic activity of these complexes has often been investigated in organic solvents and chemical reducing agents are typically used.<sup>25-29</sup> These reaction conditions do not resemble those in which the ORR activity of MCOs has been studied.

On the other hand, electrochemical studies that have reported the ORR activity of homogeneous metal complexes with two<sup>30-32</sup> or even three<sup>31, 33, 34</sup> copper atoms in aqueous solutions all lack evidence that direct cooperativity between the copper centers takes place during catalysis. A reason for this is that covalently linking copper sites will not invariably result in synergy between the metal centers. For instance, not all metal centers might participate during catalysis,<sup>31</sup> the copper sites can turn away from each other,<sup>30</sup> the catalyst can decompose during electrocatalysis,<sup>32</sup> or multiple copper centers in close proximity will result in a change of selectivity, but not due to direct metal-metal cooperativity.<sup>33</sup> An exception is a study by Yu and co-workers, in which three copper centers are forced closely together, although a full characterization of the active species and a catalytic mechanism are absent.<sup>34</sup>

To achieve catalytic ORR in a cooperative manner, we set out to study the ORR activity of a complex with a rigid ligand framework that can coordinate two copper

atoms in close proximity. Recently, the mononuclear Cu(tpma) complex (tpma= tris(2-pyridylmethyl)amine) was studied in one of our groups, and was shown to catalyze the ORR with the highest TOF reported for any homogeneous copper complex.<sup>35</sup> Interestingly, the dinuclear analogue of tpma, the 2,7-bis[bis(2-pyridylmethyl)aminomethyl]-1,8-naphthyridine (BPMAN) ligand, can coordinate two copper atoms in close proximity to form the  $[\text{Cu}_2\text{L}(\mu\text{-OH})]^{3+}$  ( $\text{L} = \text{BPMAN}$ ) complex<sup>36</sup> and was previously reported to electrochemically catalyze the water oxidation reaction.<sup>37</sup> It is evident from **Figure 4.1** that  $[\text{Cu}_2\text{L}(\mu\text{-OH})]^{3+}$  bears similarities to the T3 site in MCOs, including the  $\mu\text{-OH}$  ligand. Moreover, the Cu–Cu distance in  $[\text{Cu}_2\text{L}(\mu\text{-OH})]^{3+}$  was reported to be 3.4 Å,<sup>37</sup> which is similar to the reported Cu–Cu distance in the T3 site of MCOs in the RO state of approximately 3.7 Å.<sup>12</sup>

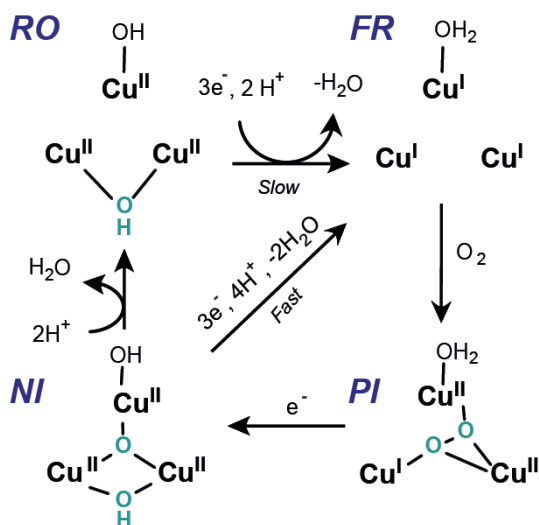


**Figure 4.2** Schematic overview of the oxygen reduction mechanism in the TNC of MCOs.

In this study, we present a mechanistic investigation of the ORR catalyzed by  $[\text{Cu}_2\text{L}(\mu\text{-OH})]^{3+}$  and explain its activity and selectivity, which is supported by a combination of electrochemical and reactivity studies to identify the nature of the active species. In addition, by comparing our results to the previously reported mononuclear Cu(tpma) system, the effect of the dinuclear copper core on the reaction kinetics and selectivity was explored. In this way, the study of this T3 site-inspired complex contributes to better understanding of how the cooperative function of multiple metals in close proximity can affect ORR activity and selectivity.

## 4.2 Results and Discussion

### 4.2.1 Synthesis of $[\text{Cu}_2\text{L}(\mu\text{-OH})]\text{OTf}_3$

The 2,7-bis[bis(2-pyridylmethyl)aminomethyl]-1,8-naphthyridine ligand was synthesized using a new synthetic protocol (see **Appendix C.1**). With the BPMAN ligand (**L**) in hand, crystalline  $[\text{BPMANCu}_2(\mu\text{-OH})](\text{OTf})_3$  ( $[\text{Cu}_2\text{L}(\mu\text{-OH})]\text{OTf}_3$ ) was prepared in a reaction with  $\text{Cu}(\text{OTf})_2$  in acetonitrile according to literature procedures.<sup>37</sup> The paramagnetic  $^1\text{H-NMR}$  spectrum of  $[\text{Cu}_2\text{L}(\mu\text{-OH})]^{3+}$  in  $\text{D}_2\text{O}$ , not reported previously, shows a set of 7 and a set of 2 of equally integrating resonances between +71 and +8 ppm with a relative ratio of 2:1 (see **Figure C.3**). This observation can be explained by the methylene protons flanking the pendant pyridines being magnetically inequivalent (set of 2) and agrees with the expected resonances of the four pyridine arms and the 1,8-naphthyridine moiety. The surprisingly sharp peaks in the paramagnetic  $^1\text{H-NMR}$  spectrum of this dicopper(II) compound are likely the result of antiferromagnetic coupling between the two Cu(II) centers, as has been observed for other hydroxo-bridged dicopper(II) complexes.<sup>38, 39</sup> The paramagnetic  $^1\text{H-NMR}$  spectrum of the same compound in  $\text{DCM-d}_2$  gives rise to a similar spectrum, except for an additional broad resonance at -70.8 ppm (**Figure C.5**). We assign this resonance to the hydroxide proton and attribute the absence of this resonance in  $\text{D}_2\text{O}$  to rapid exchange of the proton with the solvent.

### 4.2.2 Cyclic voltammetry of $[\text{Cu}_2\text{L}(\mu\text{-OH})]\text{OTf}_3$

The  $[\text{Cu}_2\text{L}(\mu\text{-OH})]^{3+}$  complex was studied electrochemically in a 0.1 M phosphate buffer (PB) at pH 7, using a glassy carbon (GC) working electrode. A cyclic voltammogram (CV) under Ar atmosphere shows a single  $\text{Cu}^{\text{II}}/\text{Cu}^{\text{I}}$  redox couple with a half-wave potential ( $E_{1/2}$ ) of 0.45 V vs. RHE (**Figure 4.3a**). The redox couple of  $[\text{Cu}_2\text{L}(\mu\text{-OH})]^{3+}$  is shifted towards higher potentials compared to the mono-nuclear analogue  $\text{Cu}(\text{tmpa})$  that has a  $E_{1/2}$  of 0.21 V vs. RHE under the same conditions.<sup>35</sup> To investigate if  $[\text{Cu}_2\text{L}(\mu\text{-OH})]^{3+}$  displays ORR activity, a CV in the presence of oxygen was recorded. Indeed, the CV showed a clear catalytic wave (**Figure 4.3b**). In addition to the ORR, the catalytic activity of  $[\text{Cu}_2\text{L}(\mu\text{-OH})]^{3+}$  for the hydrogen peroxide reduction reaction (HPRR) is of interest because  $\text{H}_2\text{O}_2$  is found as a detectable intermediate in the aqueous electrochemical ORR mechanism of other copper complexes with tetradentate pyridylamine ligands that is formed after the two-electron reduction of oxygen.<sup>30, 33, 35, 40, 41</sup> In the presence of 1.1 mM  $\text{H}_2\text{O}_2$ , which is the same concentration as the maximum solubility of oxygen in PB, a catalytic wave was observed with a slightly earlier onset

than the ORR (**Figure 4.3b**). As this earlier onset is only present in the first scan, we contribute this occurrence to the weak binding of  $\text{H}_2\text{O}_2$  to the oxidized form of the catalyst, although such a species could not be detected by other techniques like NMR. As the time between the first and second scan is relatively short, this equilibrium is not restored in between cycles and the onset shifts back to that of the ORR in subsequent scans (**Figure C.7**). The peak-shaped waves in both the ORR and HPRR voltammograms indicate the depletion of substrate during catalysis. The same mass transfer phenomena are observed in rotating disk electrode experiments, *vide infra*. We attribute the difference in the peak catalytic currents between the the ORR and HPRR to the different diffusion rates of  $\text{O}_2$  ( $1.9 \times 10^{-5} \text{ cm}^2 \text{ s}^{-1}$ ) and  $\text{H}_2\text{O}_2$  ( $0.8 - 1.4 \times 10^{-5} \text{ cm}^2 \text{ s}^{-1}$ )<sup>42, 43</sup> and possible difference in electron transfer number for each of the respective reduction reactions.

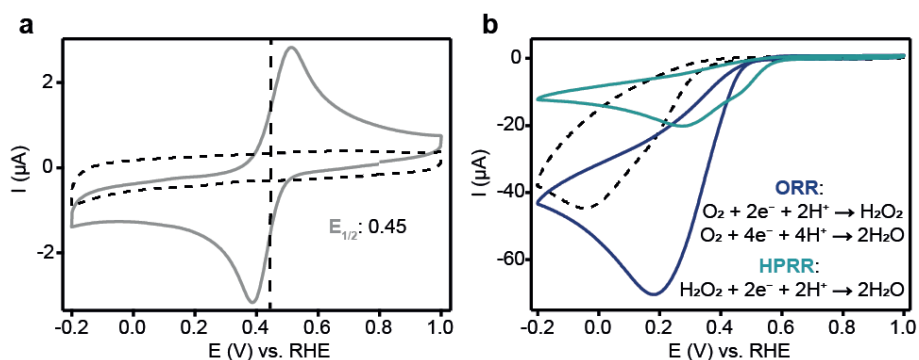


**Figure 4.3** CVs of **a**) the  $\text{Cu}^{\text{II}}/\text{Cu}^{\text{I}}$  redox couple of  $[\text{Cu}_2\text{L}(\mu\text{-OH})]^{3+}$  with the half-wave potential of 0.45 V vs. RHE indicated by the vertical line and the bare GC electrode under Ar atmosphere by a black dashed line, and **b**) the ORR (dark blue) and HPRR (light blue) catalysed by  $[\text{Cu}_2\text{L}(\mu\text{-OH})]^{3+}$ . ORR activity of the bare GC electrode shown as reference (black dashed line). Conditions: 0.15 mM  $[\text{Cu}_2\text{L}(\mu\text{-OH})]^{3+}$ , 0.1 M PB pH 7, Ar or  $\text{O}_2$  atmosphere or 1.1 mM  $\text{H}_2\text{O}_2$ , 293 K, 100 mV/s scan rate.

Prior to further mechanistic studies, we carefully investigated if the electrochemical data is representative of the homogenous catalyst in solution, rather than any heterogeneous species that may have been deposited on the electrode surface. Such investigation on the nature and stability of the active species is important in homogeneous electrocatalysis.<sup>44</sup> This has been exemplified by a previous study by one of our groups on a different dicopper ORR catalyst used as a model system for MCOs, for which the sole active species in ORR was found to be copper deposit.<sup>32</sup> In addition, catalytic rates and selectivities can only be assigned to the homogeneous catalyst in solution if the interference of any formed heterogeneous deposits can be minimized.

The possible formation of any deposited species was studied in a combination of CV experiments and electrochemical quartz crystal microbalance (EQCM) experiments (**Appendix C.3**). First, we investigated if any species deposits onto the electrode during CV measurements, by recording a CV in a solution of  $[\text{Cu}_2\text{L}(\mu\text{-OH})]^{3+}$ , and subsequently recording a CV of the same electrode in a solution in the absence of catalyst. These experiments under Ar atmosphere show that the  $[\text{Cu}_2\text{L}(\mu\text{-OH})]^{3+}$  catalyst tends to adsorb onto the glassy carbon electrode during CV measurements, but it is likely to stay intact as the redox couple of the species that adsorbs onto the electrode has the same  $E_{1/2}$  as the  $[\text{Cu}_2\text{L}(\mu\text{-OH})]^{3+}$  redox couple (**Figure C.8a**, **Figure C.9a**). In contrast, the same experiments in the presence of  $\text{O}_2$  or  $\text{H}_2\text{O}_2$  show that a new heterogeneous species forms on the electrode during catalysis that is also catalytically active for the ORR and HPRR (**Figure C.8**). This indicates that the catalyst partly decomposes during catalysis. Furthermore, EQCM measurements were carried out to investigate the possible mass change of the electrode during CV experiments, as this is an indication that heterogeneous deposits form on the surface of the electrode. In line with the CV experiments discussed above, EQCM experiments indeed show that a heterogeneous species is formed on the surface of the electrode during catalysis, whereas this formation is prevented if the  $[\text{Cu}_2\text{L}(\mu\text{-OH})]^{3+}$  catalyst is studied under Ar atmosphere (**Figure C.12**).

Next, we investigated to what extent the adsorption of catalyst or the formation of a deposit on the electrode surface contribute to the recorded activity of  $[\text{Cu}_2\text{L}(\mu\text{-OH})]^{3+}$ . In measurements under Ar atmosphere the adsorbed species behaves similar to the homogenous one, and upon changing to oxygen atmosphere its catalytic activity is small as only a little amount of catalyst adsorbs onto the electrode (see **Figure C.9** and **Figure C.10a**). Therefore, it was excluded that any adsorbed catalyst interferes with the measurements of the homogeneous  $[\text{Cu}_2\text{L}(\mu\text{-OH})]^{3+}$  species under Ar atmosphere.

To study the catalytic activity of the deposit that forms during catalysis by decomposition of  $[\text{Cu}_2\text{L}(\mu\text{-OH})]^{3+}$ , additional measurements were carried out under non-substrate limited conditions. These conditions allow to study the catalytic activity, whilst this is not governed by the depletion of oxygen. From these measurements, it is clear that the catalytic activity of  $[\text{Cu}_2\text{L}(\mu\text{-OH})]^{3+}$  in the first scan of a CV measurement is significantly less than the activity of the deposits that form over the course of several scans (**Figure C.10a**). In other words, under catalytic conditions, active deposits form over the course of multiple CV scan. To verify that the largest part of the activity can still be contributed to the homogeneous  $[\text{Cu}_2\text{L}(\mu\text{-OH})]^{3+}$  species, we investigated the activity of the deposit that forms only during the first part of the catalytic CV measurement (**Figure C.11**). This indicates that the contribution of the deposit to the

catalytic current is minimal, which is further supported by the EQCM measurements that show that the buildup of material on the electrode predominantly occurs below 0.2 V, when the ORR has already peaked under stationary conditions.

To ensure that the influence of any heterogeneous deposits on the results of our studies into the activity of homogeneous  $[\text{Cu}_2\text{L}(\mu\text{-OH})]^{3+}$  is kept to a minimum, in this work only the first CV scans recorded on a freshly polished electrode were used. In addition, this study focusses solely on the fundamental catalytic mechanism of the catalyst, not on any long-term activity, since in that case the influence of heterogeneous deposits cannot be ruled out.

### 4.2.3 Redox behavior of $[\text{Cu}_2\text{L}(\mu\text{-OH})]\text{OTf}_3$

The first step in the catalytic ORR mechanism is the reduction of  $[\text{Cu}_2\text{L}(\mu\text{-OH})]^{3+}$  to obtain the active reduced catalyst. The redox behavior of  $[\text{Cu}_2\text{L}(\mu\text{-OH})]^{3+}$  was previously investigated by Zhang *et al.* in 0.1 M PB of pH 7 using a boron-doped diamond (BDD) working electrode. They reported two irreversible waves for the reduction and oxidation of the catalyst with a peak-to-peak separation ( $\Delta E_p$ ) of 340 mV at a scan rate of 5 mV/s. In our study, the  $\Delta E_p$  of the  $\text{Cu}^{\text{II}}/\text{Cu}^{\text{I}}$  redox couple at a scan rate of 100 mV/s reduces to 127 mV (**Figure 4.3**). We attribute the smaller  $\Delta E_p$  in this study to the more favorable electron transfer properties of GC compared to BDD, as BDD is known to act as a semi-conductor at low dopant densities.<sup>45</sup>

Scan rate dependence studies of the redox couple (10-500 mV/s) show that the peak current linearly depends on the square root of the scan rate, which indicates a diffusion-controlled process and hence that  $[\text{Cu}_2\text{L}(\mu\text{-OH})]^{3+}$  is present as a homogeneous species in solution (see **Figure C.13b**). The  $\Delta E_p$  of 127 mV at 100 mV/s indicates a quasi-reversible process and suggests that the electron transfer process to reduce and re-oxidize  $[\text{Cu}_2\text{L}(\mu\text{-OH})]^{3+}$  is slow. In addition, a Laviron plot shows that the peak potential of the redox couple depends linearly on the logarithm of the scan rate (see **Figure C.13c**), which means that the electron transfer processes in the catalyst become relatively slow compared to the timescale of the CV experiment. A third sign of slow electron transfer kinetics is the relatively low half-wave potential of the catalytic wave ( $E_{\text{cat}/2}$ ) in the ORR and thus  $E_{\text{cat}/2} < E_{1/2}$  holds for  $[\text{Cu}_2\text{L}(\mu\text{-OH})]^{3+}$ , while for fast catalysts it is expected that  $E_{\text{cat}/2} = E_{1/2}$  or even  $E_{\text{cat}/2} > E_{1/2}$ , when substrate depletion plays a role.

In MCOs, both copper centers in the T3 site of the RO state are reduced simultaneously in a proton-coupled electron transfer (PCET) step to form the FR state, resulting in the loss of the  $\mu$ -hydroxyl ligand as  $\text{H}_2\text{O}$ .<sup>6, 11</sup> In this study only a single peak for the  $\text{Cu}^{\text{II}}/\text{Cu}^{\text{I}}$  redox couple is observed, which indicates that in  $[\text{Cu}_2\text{L}(\mu\text{-OH})]^{3+}$  both copper atoms are reduced and oxidized simultaneously. To see whether the reduction

of  $[\text{Cu}_2\text{L}(\mu\text{-OH})]^{3+}$  also involves a protonation, we studied the influence of the proton concentration on the redox behavior of the complex (see **Section C.5**). CVs of  $[\text{Cu}_2\text{L}(\mu\text{-OH})]^{3+}$  under Ar atmosphere were recorded in a 0.01 M Britton-Robinson buffer over a wide pH range. Attempts to study the pH dependence in unbuffered solution resulted in difficulties in obtaining reproducible data. We ascribe this observed irregularity to the complex's propensity to access different protonation states. Particularly, the pyridinic nitrogen atoms of the ligand can be protonated easily as shown computationally by Zhang *et al.*<sup>37</sup> The use of a buffered solution minimizes local pH changes during experiments. CV measurements in buffered solution show that the  $E_{1/2}$  of the  $[\text{Cu}_2\text{L}(\mu\text{-OH})]^{3+}$  redox couple changes as a function of pH. The slope of this graph is -17 mV/dec, which we could not assign to a specific reaction step involving one or more protons (**Figure C.14b**).

More clarity was obtained from analysis of differential pulse voltammetry (DPV) measurements at varying pH, a technique that can deconvolute multiple redox events (**Figure C.15**). A plot of the peak potential of the cathodic ( $E_{pc}$ ) and anodic ( $E_{pa}$ ) events as a function of pH, shows that both peaks shift in a different manner upon changing the pH (**Figure 4.4**). Between pH 4 and 7, the reductive peak changes with -26 mV/dec. This value is close to the theoretical value of -30 mV/decade of a step in which one proton and two electrons are transferred,<sup>46</sup> and agrees with the protonation of the hydroxyl ligand upon reduction of both copper centers in  $[\text{Cu}_2\text{L}(\mu\text{-OH})]^{3+}$ . In contrast, Zhang *et al.* measured on BDD a shift of -60 mV/decade of the cathodic wave, which they contributed to the single electron reduction of  $[\text{Cu}_2\text{L}(\mu\text{-OH})]^{3+}$  and a proton transfer forming a mixed-valence  $\text{Cu}^{\text{II}}\text{Cu}^{\text{I}}$  species.<sup>37</sup> Our results differ from this observation, likely due to the more favorable electron transfer rates featured by the GC electrode. Above pH 7, a clear kink in the graph can be seen and the cathodic peak shifts with only -17 mV/dec. This points towards a mechanism in which mainly electrons are transferred, and suggests that under alkaline conditions the  $\mu$ -hydroxyl ligand is not always protonated before it will leave the copper site.

Regarding the anodic peak, we observe a trend that is the opposite of the cathodic peak. At low pH, the position of the oxidation peak does not change, while above pH 7 we observe a slope of -35 mV/dec. At these high pH values, we ascribe this slope to the formation of either a bis- $\mu$ -hydroxyl or deprotonated  $\mu\text{-O}$  species.

Interestingly, the oxidative DPV measurement at low pH values gives rise to a second oxidation peak at more positive potentials (**Figure C.15b**). The presence of a second oxidation peak which only forms at low pH values suggests that at a high proton concentration induces a chemical process. We could not further verify the origin of this

second oxidation peak, but hypothesize it belongs to oxidation of a slow equilibrium product that forms out of  $\text{Cu(I)Cu(I)}$ .

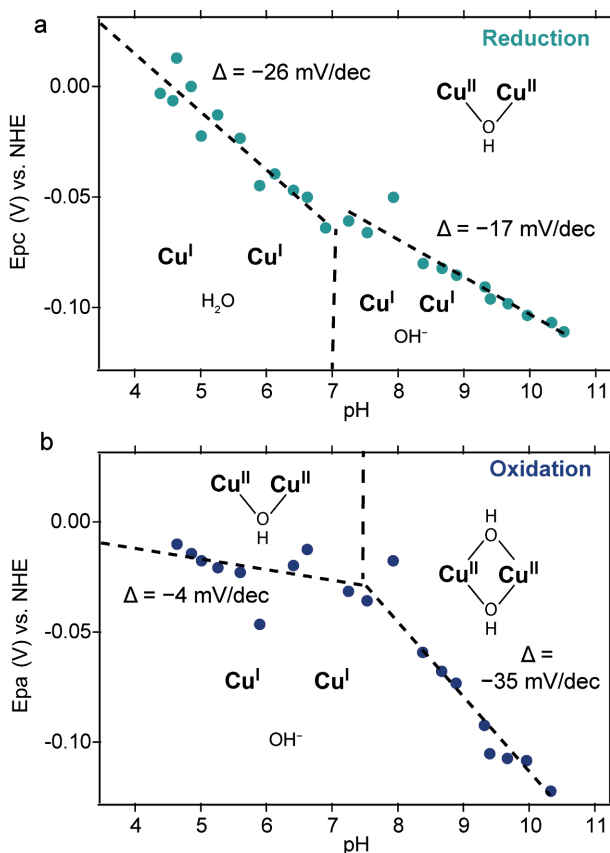


**Figure 4.4** Plot of the peak potential of a) the cathodic ( $E_{\text{pc}}$ ) and b) anodic ( $E_{\text{pa}}$ ) peaks of  $[\text{Cu}_2\text{L}(\mu\text{-OH})]^{3+}$  from DPV measurements as a function of pH, including the slope of the graph and the different dicopper species involved in the processes. Conditions: 0.15 mM  $[\text{Cu}_2\text{L}(\mu\text{-OH})]^{3+}$ , 0.01 M Britton-Robinson buffer and 0.05 M  $\text{Na}_2\text{SO}_4$ , Ar atmosphere, 293 K, DPV recorded with regular voltage pulses of 3 mV, a step potential of 0.3 mV, a modulation time of 3 ms, and a time interval of 50 ms.

The redox behavior of  $[\text{Cu}_2\text{L}(\mu\text{-OH})]^{3+}$  was also studied in acetonitrile solution since precise control over the availability of protons is more easily attainable in organic solvent than in aqueous solution. Interestingly, a solution of 0.3 mM  $[\text{Cu}_2\text{L}(\mu\text{-OH})]^{3+}$  in 0.1 M  $\text{TBAPF}_6$  in MeCN does not show a clear reduction event, which is not in agreement with the single reduction peak observed in aqueous solutions (see **Section 4.2.4**). The multiple, small reduction peaks observed below -0.5 V vs. RHE could not be assigned to a specific redox process, and most likely are the result of traces of water

that are always present in MeCN. Addition of a proton source (triethylammonium hexafluorophosphate, TEAPF<sub>6</sub>) generates a CV with a clear redox couple and a single reduction wave, demonstrating that in MeCN a proton source is required for the reduction of [Cu<sub>2</sub>L(μ-OH)]<sup>3+</sup>. Such behavior is expected in organic solutions as it is likely that upon reduction of the catalyst formation of H<sub>2</sub>O is preferred over the liberation of OH<sup>-</sup>. This agrees with the observations in aqueous solution below pH 7 and strongly suggests that protonation of the μ-hydroxyl ligand takes place simultaneously with reduction of the catalyst.

#### 4.2.4 The role of the bridging hydroxyl ligand

Intrigued by the complex redox behavior of [Cu<sub>2</sub>L(μ-OH)]<sup>3+</sup>, the coordination chemistry of the Cu<sup>II</sup>-OH-Cu<sup>II</sup> motif was studied in more detail. To begin with, possible protonation of the μ-hydroxyl ligand was studied in UV-vis measurements. The absorption band at 350 nm gradually disappears when the pH is lowered from 5.8 to 2.8 and reappears again when the pH is increased. Based on literature, we expect this absorption to be the OH<sup>-</sup> → Cu(II) LMCT.<sup>47</sup> We ascribe this change to the protonation of the hydroxide and the reversible formation of a [Cu<sub>2</sub>L(H<sub>2</sub>O)]<sup>4+</sup> complex (see **Figure C.16**).

To further gain insight into the Cu<sup>II</sup>-OH-Cu<sup>II</sup> motif, it was studied how the μ-hydroxyl ligand can form (see **Figure 4.5**). Attempts to synthesize the [Cu<sub>2</sub>L](OTf)<sub>4</sub> complex did not succeed. In the presence of trace amounts of water the [Cu<sub>2</sub>L(μ-OH)]<sup>3+</sup> species will form, which points out that the μ-hydroxyl ligand results in the formation of a very stable Cu(II) species. Therefore, the Cu<sup>I</sup> complex [Cu<sub>2</sub>L](OTf)<sub>2</sub> was synthesized from treatment of BPMAN with 1 equivalent of [CuOTf]<sub>2</sub>·toluene in DCM in 97% yield with NMR data agreeing with reported literature values (see **Appendix C**).<sup>36</sup> To see whether the bridging hydroxyl ligand can form, a solution of [Cu<sub>2</sub>L]<sup>2+</sup> in DCM was exposed to air. This resulted in conversion towards a new, green colored species, which gives rise to a set of paramagnetic resonances in the <sup>1</sup>H-NMR spectrum that match the resonances found for [Cu<sub>2</sub>L(μ-OH)]<sup>3+</sup> (Spec. Yield= 29%, see **Appendix C.6.1**). Interestingly, within two minutes of exposing the DCM solution to air a short-lived (only trace amounts detectable after 1h) intermediate was observed in the <sup>1</sup>H-NMR spectrum. We argue that the intermediate we observe in NMR is not the previously spectroscopically observed μ-1,2-peroxide, which was reported to be short-lived even at -78 °C.<sup>36</sup> Instead, the observed intermediate could be one of the dicopper(II) species along the possible sequence of the hydroperoxo, and oxo intermediates leading up to the formation of [Cu<sub>2</sub>L(μ-OH)]<sup>3+</sup>. Dicopper(II) μ-O species are highly basic<sup>48</sup> and are capable of abstracting a proton from introduced moisture, the solvent or one of the benzylic positions of the ligand. Alternatively, C-H activation of the benzylic hydrogens by the

transient Cu(II) peroxy is also a possibility. The abstraction of a proton or hydrogen from the benzylic positions of the BPMAN ligand is also in agreement with the low spectroscopic yield of 29% found for this reaction and the progressive color change of the mixture to dark orange overnight. To probe this hypothesis further, a DCM solution of  $[\text{Cu}_2\text{L}]^{2+}$  was treated with 1 equivalent of the oxo transfer agent iodossylbenzene (PhIO) under anaerobic conditions, which resulted in the formation of a progressively darker orange reaction mixture. Analysis of the  $^1\text{H-NMR}$  spectrum of this mixture revealed  $[\text{Cu}_2\text{L}(\mu\text{-OH})]^{3+}$  as the only observable species in a spectroscopic yield of 14% (see **Section C.6.2**). Reforming  $[\text{Cu}_2\text{L}](\text{OTf})_2$  out of  $[\text{Cu}_2\text{L}(\mu\text{-OH})](\text{OTf})_3$  is also possible by sequentially treating a THF suspension of  $[\text{Cu}_2\text{L}(\mu\text{-OH})](\text{OTf})_3$  with 2 equiv of  $\text{Co}(\text{Cp}^*)_2$  and an equivalent of pyridinium triflate (see **Section C.6.3**).

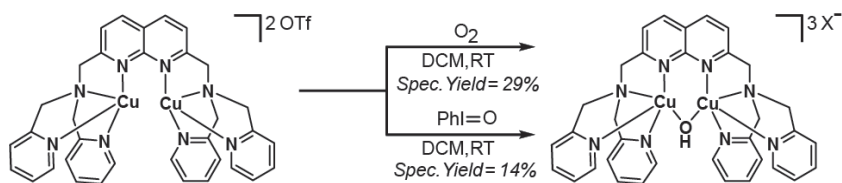


**Figure 4.5** Overview of the reactions taking place when a solution of the  $[\text{Cu}_2\text{L}](\text{OTf})_2$  complex in DCM is exposed to air or to PhIO, resulting in the formation of the oxidized  $[\text{Cu}_2\text{L}(\mu\text{-OH})]^{3+}$  cation in low spectroscopic yields.

Next, the aptitude of the reduced  $[\text{Cu}_2\text{L}](\text{OTf})_2$  complex to form the  $\text{Cu}^{\text{II}}\text{-OH-Cu}^{\text{II}}$  motif was confirmed in electrochemical experiments as well. The redox couple of  $[\text{Cu}_2\text{L}]^{2+}$ , lacking the  $\mu$ -hydroxyl ligand, was recorded in acetonitrile solution under inert conditions showing that the oxidized  $[\text{Cu}_2\text{L}]^{4+}$  complex can be formed in acetonitrile. (**Figure 4.6b**). From these measurements it is evident that the reduction and oxidation peak of  $[\text{Cu}_2\text{L}]^{2+}$  shifted to more positive potentials compared to the  $\text{Cu}^{\text{II}}\text{-OH-Cu}^{\text{II}}$  species, as the  $E_{1/2}$  of  $[\text{Cu}_2\text{L}]^{2+}$  is  $-0.33$  V vs. Fc and the  $E_{1/2}$  of  $[\text{Cu}_2\text{L}(\mu\text{-OH})]^{3+}$  is  $-0.48$  V vs. Fc. In addition, the redox couple of  $[\text{Cu}_2\text{L}]^{2+}$  is more reversible than of  $[\text{Cu}_2\text{L}(\mu\text{-OH})]^{3+}$ , which is an indication that in absence of the bridging hydroxyl ligand the electron transfer and reorganization between the  $\text{Cu}^{\text{I}}\text{-Cu}^{\text{I}}$  and  $\text{Cu}^{\text{II}}\text{-Cu}^{\text{II}}$  species becomes easier. Moreover, these observations suggest that the negatively charged  $\mu$ -hydroxyl ligand stabilizes the oxidized dinuclear copper core in  $[\text{Cu}_2\text{L}(\mu\text{-OH})]^{3+}$  and that there is a thermodynamic driving force to form this ligand (**Figure 4.6b-c**).

In the same experiment in water, it is possible for  $\text{OH}^-$  to bind to the dicopper core when  $[\text{Cu}_2\text{L}]^{2+}$  is oxidized or exposed to oxygen, and  $[\text{Cu}_2\text{L}(\mu\text{-OH})]^{3+}$  instead of  $[\text{Cu}_2\text{L}]^{4+}$  forms (see **Figure C.27**). Interestingly, exposure of the  $[\text{Cu}_2\text{L}]^{2+}$  acetonitrile solution to oxygen from the air will form the  $[\text{Cu}_2\text{L}(\mu\text{-OH})]^{3+}$  species only when a proton source is

added, while the complex seems to undergo decomposition to unidentified species when no source of protons is available (see **Appendix C.7**). It is to be expected that this decomposition is caused by the abstraction of a proton from the ligand, which agrees with the observed reactivity described in the previous section. In this way, the reactivity studies and electrochemical experiments show good agreement, and together highlight the fast formation of the  $\mu$ -hydroxyl ligand if the complex is in the presence of both an oxygen and a proton source.

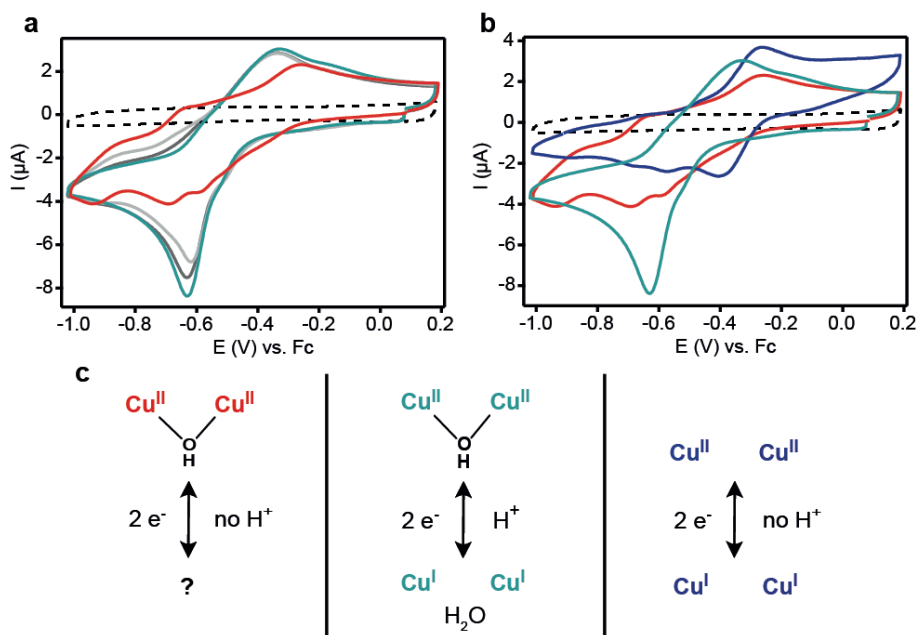


**Figure 4.6** a) CVs of 0.3 mM  $[\text{Cu}_2\text{L}(\mu\text{-OH})]^{3+}$  with no (red), 0.15 mM (light grey), 0.6 mM (dark grey), and 1.0 mM (light blue)  $\text{TEAPF}_6$  present. b) CVs of 0.3 mM  $[\text{Cu}_2\text{L}(\mu\text{-OH})]^{3+}$  with (light blue) and without (red) 1.0 mM  $\text{TEAPF}_6$  compared to the 0.3 mM  $[\text{Cu}_2\text{L}]^{2+}$  redox couple (dark blue). c) Schematic overview of the redox processes taking place in figure b). Conditions: 0.1 M  $\text{TBAPF}_6$  in MeCN, Ar atmosphere, 293 K, 100 mV/s scan rate.

#### 4.2.5 Reaction kinetics of the ORR and HPRR

To get insight into the catalytic mechanism that follows upon reduction of  $[\text{Cu}_2\text{L}(\mu\text{-OH})]^{3+}$ , catalyst concentration dependencies were determined for the ORR and HPRR (**Figure 4.7a-b**). These dependencies were studied in the regime of low catalyst concentrations (1–4  $\mu\text{M}$ ), where the reaction rates are not limited by substrate. For the HPRR this leads to CV measurements that resemble a plateau current, which is an indication that the reaction is not controlled by diffusion of substrate. In case of the

ORR, we were not able to observe plateau-like currents, although we do see a dependence of the catalytic current on the catalyst concentration. Hence, we assume that our measurements are not fully dominated by substrate consumption. Additionally, the H<sub>2</sub>O<sub>2</sub> concentration was varied to determine the reaction dependency in substrate (**Figure 4.7c-d**). Since a clear catalytic plateau was absent, the dependence in H<sub>2</sub>O<sub>2</sub> concentration was determined at a potential of 0.2 V vs. RHE. In both the ORR and HPRR a linear first-order dependence of the catalytic current on the catalyst concentration was observed. In addition, a first-order dependence of the catalytic current on the substrate concentration for the HPRR was observed. For the ORR the substrate dependence was not determined, although we assume that in the same manner one molecule of oxygen at a time will react at the dinuclear copper site.

Next, the same experiments were used to gain insight into the reaction kinetics. For low concentrations of [Cu<sub>2</sub>L(μ-OH)]<sup>3+</sup>, the reaction is not limited by substrate availability and a quantitative value for the observed rate constant (*k*<sub>obs</sub>) can be determined from the catalytic current enhancement method using **Equation 4.1**.<sup>49, 50</sup>

$$\frac{i_{cat}}{i_p} = 2.24n \sqrt{\frac{RT}{Fv}} k_{obs} \quad (4.1)$$

This equation holds for electrochemical processes which are controlled by a rate-limiting chemical step, and wherein no intermolecular electron transfer steps take place. In **Equation 4.1**, *i*<sub>cat</sub> is the measured catalytic current, *i*<sub>p</sub> is the peak current in absence of substrate, *n* is the number of electrons transferred in the catalytic reaction, *T* is the temperature (*T* = 293 K), *v* is the scan rate (*v* = 100 mV/s) and *k*<sub>obs</sub> is the observed first-order rate constant. The theoretical *i*<sub>p</sub> was calculated from the Randles-Sevcik equation, because of the low catalyst concentrations (**Appendix C.4**). It is not possible to determine the number of electrons transferred in the ORR from stationary CV experiments, hence we determined the *k*<sub>obs</sub> for the ORR as the range between the minimum number of electrons transferred to reduce oxygen to H<sub>2</sub>O<sub>2</sub> (*n*=2) and the complete reduction of oxygen to water (*n*=4). The calculated values for *k*<sub>obs</sub> from the current enhancement method lie between  $3.7 \pm 1.0 \times 10^3 \text{ s}^{-1}$  and  $14.7 \pm 4.2 \times 10^3 \text{ s}^{-1}$  for the ORR and is  $4.8 \pm 1.4 \times 10^3 \text{ s}^{-1}$  for the HPRR (**Appendix C.8**). It should be noted that the *k*<sub>obs</sub> values for the ORR were determined under conditions that might not be under kinetic control. For that reason, care should be taken not to overinterpret the results and a comparison between the found *k*<sub>obs</sub> values for the ORR and HPRR may be invalid, given that the *k*<sub>obs</sub> for ORR is probably underestimated.

Interestingly, determination of the *k*<sub>obs</sub> for [Cu<sub>2</sub>L(μ-OH)]<sup>3+</sup> in the same manner in acetate buffer of pH 4.8 resulted in a *k*<sub>obs</sub> for the HPRR that is comparable with the value

at pH 7, whereas the  $k_{\text{obs}}$  for the ORR became almost four times as large (see **Table C.2**). This observation indicates that the  $k_{\text{obs}}$  of the ORR is proton dependent. A logical explanation for the larger  $k_{\text{obs}}$  of the ORR under acidic conditions, is that the RDS involves a protonation step, which suggests that the protonation involved in the reduction of  $[\text{Cu}_2\text{L}(\mu\text{-OH})]^{3+}$  is the RDS of the ORR. The fact that the  $k_{\text{obs}}$  of the HPRR is not influenced by the pH can be explained by the fact that after reduction of the catalyst, the HPRR mechanism is followed by another slow step that does not lead to a general increase of the observed rate.

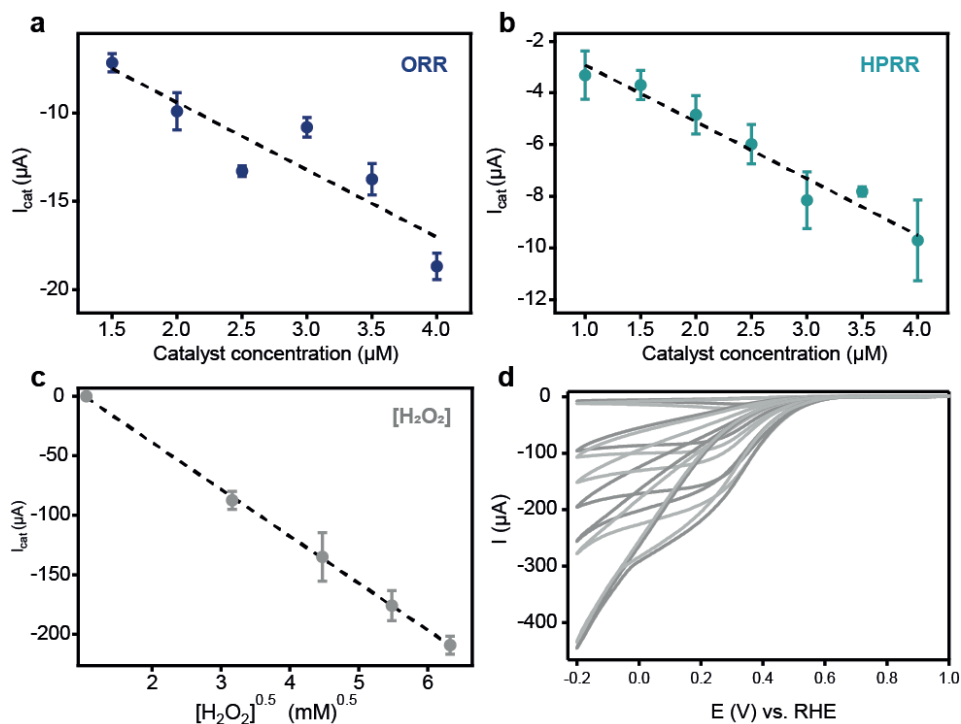


**Figure 4.7** The background-corrected catalytic currents plotted against the a) catalyst concentration for the ORR, b) catalyst concentration for the HPRR (1.1 mM  $\text{H}_2\text{O}_2$ ), c) square root of the  $\text{H}_2\text{O}_2$  concentration for the HPRR at 0.2 V vs. RHE (0.15 mM  $[\text{Cu}_2\text{L}(\mu\text{-OH})]^{3+}$ ) and d) the CVs of the HPRR corresponding to figure c. In figure a-c, the data points are the average of two measurements. Conditions: 0.1 M PB pH 7, Ar or  $\text{O}_2$  atmosphere, 293 K, 100 mV/s scan rate

#### 4.2.6 Further insight into the HPRR mechanism

Intrigued by the proton-independent  $k_{\text{obs}}$  of the HPRR, we further investigated the reaction mechanism. First, a solvent kinetic isotope effect (KIE) of  $1.08 \pm 0.25$  for the HPRR was determined under non-substrate limiting conditions (**Appendix C.9**). This value indicates either the absence of a KIE, or the presence of a minor secondary KIE,

suggesting that the RDS of the reaction indeed does not involve breaking of an O-H bond. Such a small KIE is in contrast with the previously determined KIE of Cu(tmpa) for the HPRR of 1.4-1.7, which was proposed to go through a Fenton-type mechanism, producing radical species upon homolytical cleavage of the O-O bond.<sup>51</sup> To exclude such a Fenton-type mechanism for  $[\text{Cu}_2\text{L}(\mu\text{-OH})]^{3+}$ , hydroxyl radical trapping experiments for the HPRR were carried out during which no radicals could be detected (see **Appendix C.10**).

Interestingly, exposing a degassed  $\text{D}_2\text{O}$  suspension of  $[\text{Cu}_2\text{L}]^{2+}$  to an equivalent of  $\text{H}_2\text{O}_2$  led to the instant formation of a green, water-soluble species that gave rise to a different paramagnetic  $^1\text{H-NMR}$  spectrum than found for  $[\text{Cu}_2\text{L}(\mu\text{-OH})]^{3+}$  (**Appendix C.6.4**). Additionally, two absorption bands arose in the UV-Vis spectrum at 620 and 660 nm after the reaction of  $[\text{Cu}_2\text{L}]^{2+}$  with  $\text{H}_2\text{O}_2$  (**Figure C.23**). These two observations suggest that oxidation of the Cu centers to Cu(II) has occurred. The difference in NMR spectra raised the question as to what might be bound to the copper centers. The oxidation of the Cu centers pointed towards cleavage of the O-O bond of  $\text{H}_2\text{O}_2$  and hinted at the fact that the species being formed might be the  $[\text{Cu}_2\text{L}(\mu\text{-OH})_2]^{2+}$  species we postulated to form at high pH regimes in the E-pH diagram. Computational studies (**Appendix C.13**) indeed show that formation of  $[\text{Cu}_2\text{L}(\mu\text{-OH})_2]^{2+}$  from  $[\text{Cu}_2\text{L}]^{2+}$  and  $\text{H}_2\text{O}_2$  is energetically favorable by approximately 38 kcal/mol. To investigate the feasibility of a bis-hydroxide complex, we exposed a  $[\text{Cu}_2\text{L}(\mu\text{-OH})]^{3+}$  solution in  $\text{D}_2\text{O}$  to an equivalent of KOH (**Appendix C.6.5**). This indeed gave rise to the same resonances in the paramagnetic  $^1\text{H-NMR}$  spectrum as found for the reaction between  $[\text{Cu}_2\text{L}]^{2+}$  and  $\text{H}_2\text{O}_2$ . Considering the reactants in the two separate reactions and the measurements on the E-pH diagram that indicate that under basic conditions such a species can form, led us to confirm this new species as  $[\text{Cu}_2\text{L}(\mu\text{-OH})_2]^{2+}$ . The limited stability of this bis-hydroxide upon removal of the aqueous solvent however prohibited further characterization of this species. The instability of the  $[\text{Cu}_2\text{L}(\mu\text{-OH})_2]^{2+}$  species suggests that under non-basic conditions one of the  $\mu\text{-OH}$  ligands is readily protonated to produce  $[\text{Cu}_2\text{L}(\mu\text{-OH})]^{3+}$  and  $\text{H}_2\text{O}$ .

Combining the experiments on the HPRR, strong evidence is found for metal-metal cooperativity being involved in the catalytic mechanism. Firstly, there is a first order dependence of the catalytic rate on the concentration of catalyst and the concentration of  $\text{H}_2\text{O}_2$ . This validates that a single molecule of  $\text{H}_2\text{O}_2$  will be reduced at the dicopper core of the catalyst. Another observation is the fact that  $[\text{Cu}_2\text{L}(\mu\text{-OH})_2]^{2+}$  is formed when  $[\text{Cu}_2\text{L}]^{2+}$  is reacted with  $\text{H}_2\text{O}_2$ . Such a species can only form if the O-O bond is cleaved after binding of  $\text{H}_2\text{O}_2$  between both copper cores. In addition,  $[\text{Cu}_2\text{L}(\mu\text{-OH})]^{3+}$  catalyzes the HPRR via a different pathway than the mononuclear Cu(tmpa) complex.<sup>51</sup> Whereas

for Cu(tmpa) a significant KIE is observed and the mechanism is proposed to go through a Fenton-type mechanism, our experiments on  $[\text{Cu}_2\text{L}(\mu\text{-OH})]^{3+}$  exclude such a pathway. It is therefore most likely that  $[\text{Cu}_2\text{L}(\mu\text{-OH})]^{3+}$  binds  $\text{H}_2\text{O}_2$  via a different binding motif involving interactions with both copper centers, instead of end-on binding as was proposed for Cu(tmpa).<sup>51</sup>

#### 4.2.7 The selectivity of the ORR

After gaining insights into HPRR mechanism and having a strong indication that both copper centers cooperate in the binding of the  $\text{H}_2\text{O}_2$  and cleavage of the O-O bond, we set out to investigate the mechanism and cooperativity in the ORR. As stated before,  $\text{H}_2\text{O}_2$  is found as a detectable intermediate in the electrochemical ORR mechanism of other copper complexes with tetradentate pyridylamine ligands.<sup>30, 33, 35, 40, 41</sup> Hence, it is interesting to see whether the HPRR is part of the ORR occurring via two sequential 2-electron reductions, or whether  $[\text{Cu}_2\text{L}(\mu\text{-OH})]^{3+}$  can directly reduce oxygen to water via a 4-electron pathway, similar to MCOs. Therefore, rotating (ring) disk electrode (R(R)DE) experiments were employed.

First, it is important to realize that in the same manner as in stationary CV experiments, the homogeneous catalytic activity of  $[\text{Cu}_2\text{L}(\mu\text{-OH})]^{3+}$  in RRDE experiments was ensured by investigating the formation of any active deposits (**Appendix C.11.3**). Upon recording a CV in a solution of  $[\text{Cu}_2\text{L}(\mu\text{-OH})]^{3+}$ , and subsequently recording a CV of the same electrode in a blank solution that does not contain any catalyst, it was shown that a catalytically active, heterogeneous deposit forms on the electrode during the ORR. Under RRDE conditions, this deposit is less active than the homogeneous catalyst in solution (**Figure C.38a**). Next, the selectivity for the 4 or 2 electron ORR of the catalyst in solution and the formed deposits were compared, and it was shown that these experiments have a comparable outcome (**Figure C.38b**). This verifies that the formed deposits do not affect the observed selectivity of  $[\text{Cu}_2\text{L}(\mu\text{-OH})]^{3+}$ . To ensure that we exclusively study the homogeneous catalyst in solution, only the first scan of any RRDE experiment is used to assign the catalytic activity and selectivity of  $[\text{Cu}_2\text{L}(\mu\text{-OH})]^{3+}$ . In chronoamperometry measurements (CA) it is not possible to exclude contribution of any deposited species that form during the experiment. However, we do not observe any change in selectivity or activity over the course of CA experiment indicating that no build-up of a catalytically competent species occurs. An exception is when a potential close to the onset of 0.4 V vs. RHE is applied. In this case, we observe a change in the selectivity over time, which we attribute to the fact that under these conditions the current is low in general, which will easily lead to deviations in the selectivity (**Figure C.37**).

RDE CVs of  $[\text{Cu}_2\text{L}(\mu\text{-OH})]^{3+}$  recorded in PB of pH 7 at various rotation rates show slow catalysis of the ORR, because even at a strongly negative potential of  $-0.4$  V vs. RHE no clear mass-transport limited plateau is reached (see **Figure C.34**). More interestingly, RRDE measurements of  $[\text{Cu}_2\text{L}(\mu\text{-OH})]^{3+}$  were carried out to determine the selectivity of the ORR over the full potential window. In RRDE measurements the hydrogen peroxide that is produced at the GC disk can be quantified by oxidation at the Pt ring (see **Appendix C.11.2**). **Figure 4.8** shows that  $[\text{Cu}_2\text{L}(\mu\text{-OH})]^{3+}$  selectively catalyzes the four-electron ORR in both linear sweep voltammetry (LSV) and CA measurements, producing more than 70%  $\text{H}_2\text{O}$  over the main part of the potential window. Only close to the onset potential in the LSV the selectivity to  $\text{H}_2\text{O}_2$  is high, which is likely to be less accurate as the currents are (too) low. To exclude that any  $\text{H}_2\text{O}_2$  is decomposed by the catalyst before it can be detected at the ring, the stability of  $\text{H}_2\text{O}_2$  solutions in the presence of  $[\text{Cu}_2\text{L}(\mu\text{-OH})]^{3+}$  was studied. These experiments confirm that the catalyst is not capable of breaking down  $\text{H}_2\text{O}_2$  before it reaches the ring (**Appendix C.12**).

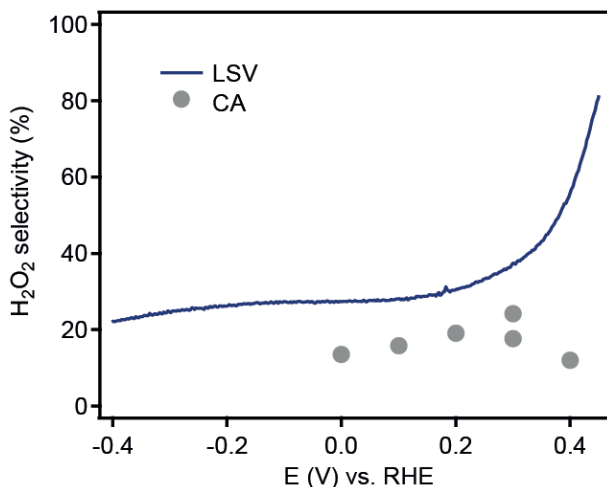


**Figure 4.8**  $\text{H}_2\text{O}_2$  selectivity of  $[\text{Cu}_2\text{L}(\mu\text{-OH})]^{3+}$  in the ORR as determined from RRDE LSV measurements (dark blue line) and CA measurements (grey dots) at different potentials. The LSV currents were corrected for the currents measured between 0.8 - 1.0 V vs. RHE and the CA points were corrected for the currents measured at 0.8 V vs. RHE preceding the experiment. Conditions: 0.15 mM  $[\text{Cu}_2\text{L}(\mu\text{-OH})]^{3+}$ ,  $\text{O}_2$  atmosphere, 0.1 M PB pH 7, 293 K, 1600 RPM, Pt ring at 1.2 V vs. RHE

It is likely that the preference of  $[\text{Cu}_2\text{L}(\mu\text{-OH})]^{3+}$  to catalyze the ORR in a four-electron process arises from metal-metal cooperativity in the dinuclear copper core. In  $[\text{Cu}_2\text{L}(\mu\text{-OH})]^{3+}$  the naphthyridine-based ligand enforces the two copper atoms to bind in close proximity and in this way facilitates bridging binding modes for exogeneous ligands, like

the peroxy intermediate.<sup>36</sup> This is in contrast with mononuclear copper complexes, that can either bind a (hydro)peroxy ligand in an end-on manner or upon reaction with oxygen will slowly dimerize to form a peroxy dicopper complex,<sup>21</sup> as is observed for Cu(tmpa).<sup>52</sup> The ORR selectivity to water of 70% by  $[\text{Cu}_2\text{L}(\mu\text{-OH})]^{3+}$  stands out compared to the selectivity of Cu(tmpa), which only converts 20% of oxygen to water in the presence of high concentrations of oxygen.<sup>35</sup> The improved selectivity of  $[\text{Cu}_2\text{L}(\mu\text{-OH})]^{3+}$  points to a different mechanism in which the enforced bridging geometries result in the thermodynamic stabilization of the formed (hydro)peroxy intermediates and facilitate the easy cleavage of the O-O bond. Furthermore, we hypothesize that the energy barrier to release any intermediate ORR products like  $\text{H}_2\text{O}_2$  from the dinuclear copper core is high. The release of  $\text{H}_2\text{O}_2$  is disfavored kinetically due to the proximal oxygen being not easily accessible for protonation. On the other hand, liberating any of the (hydro)(per)oxy ligands results in the formation of the bare dinuclear  $\text{Cu}^{\text{I}} \text{Cu}^{\text{I}}$  core, which is energetically disfavored due to severe electrostatic repulsions of the two copper centers confined in the rigid naphthyridine framework. Combined, we believe that these are the main arguments that steer the reaction to the four-electron pathway and explain the significant difference in selectivity compared to mononuclear analogues.

#### 4.2.8 Discussion of the catalytic mechanism of $[\text{Cu}_2\text{L}(\mu\text{-OH})]^{3+}$

Combining the investigations of the ORR and HPORR, a mechanism for these reactions catalyzed by  $[\text{Cu}_2\text{L}(\mu\text{-OH})]^{3+}$  could be established (**Figure 4.9**). Starting the catalytic cycle,  $[\text{Cu}_2\text{L}(\mu\text{-OH})]^{3+}$  needs to be reduced and the bridging ligand must dissociate from the dicopper core. Measurements have shown that below pH 7 two electrons and one proton are transferred and the hydroxide is released as  $\text{H}_2\text{O}$ . Under more alkaline conditions, a  $[\text{Cu}_2\text{L}(\mu\text{-OH})_2]^{2+}$  species forms that is reduced in a two electron and one proton process. In addition, CV measurements have shown that the  $\mu\text{-OH}$  moiety stabilizes the  $\text{Cu}^{\text{I}}\text{-OH}\text{-Cu}^{\text{I}}$  core, which makes activation of the catalyst harder and slows down the electron transfer in general.

After reduction and release of the bridging ligand, oxygen can bind to the  $\text{Cu}^{\text{I}} \text{Cu}^{\text{I}}$  core. From a previous study by Lippard and co-workers on the same compound, it is known that the trans- $\mu$ -1,2-peroxy species can be formed,<sup>36</sup> hence it is likely that the same species will be formed here. Next, we hypothesize that a hydroperoxy species forms after protonation. RRDE experiments show that small quantities of  $\text{H}_2\text{O}_2$  are produced during the ORR. It is speculated that the hydroperoxy can bind in a  $\mu$ -1,1 manner as such  $\mu$ -1,1-hydroperoxy species have been shown to be able to form previously,<sup>25, 53-56</sup> Although we were not able to isolate this intermediate species it is anticipated that the high selectivity of  $[\text{Cu}_2\text{L}(\mu\text{-OH})]^{3+}$  for the four-electron ORR arises

from the relatively strong binding of the (hydro)peroxy moiety between both copper atoms. This results in the four-electron ORR taking place via protonation of the distal oxygen atom and prevents formation of the disfavored bare  $\text{Cu}^{\text{II}}\text{Cu}^{\text{II}}$  species. In the next step, two electrons and two protons are transferred, resulting in cleavage of the O-O bond, and generation of  $\text{H}_2\text{O}$ . Whether this step proceeds directly or via the intermediate production of a  $\mu$ -oxo species cannot be addressed experimentally. We have shown however through our studies with the oxo-transfer agent PhIO that if an oxo-species would form it would readily be protonated, reforming  $[\text{Cu}_2\text{L}(\mu\text{-OH})]^{3+}$ .

Next to the ORR mechanism, the off-cycle HPRR mechanism was studied. After reduction of  $[\text{Cu}_2\text{L}(\mu\text{-OH})]^{3+}$ ,  $\text{H}_2\text{O}_2$  binds to the dicopper core, upon which two electrons are transferred to break the O-O bond and the  $[\text{Cu}_2\text{L}(\mu\text{-OH})_2]^{2+}$  species is formed. Due to the relative instability of this bis- $\mu$ -OH species, we hypothesize that this species will be quickly protonated to regenerate the stable  $[\text{Cu}_2\text{L}(\mu\text{-OH})]^{3+}$  complex. Though this HPRR mechanism is not part of the ORR, this reaction as well shows how having two copper centers in close proximity allows for the cooperative activation of substrates.

Altogether, the catalytic pathways of  $[\text{Cu}_2\text{L}(\mu\text{-OH})]^{3+}$  provide multiple evidence for a cooperative catalytic mechanism, which contrasts the mechanisms of previously reported dicopper-based catalysts for the electrocatalytic ORR. First of all, our studies on the reduction of  $[\text{Cu}_2\text{L}(\mu\text{-OH})]^{3+}$  and oxidation of  $[\text{Cu}_2\text{L}]^{2+}$  show that a bridging ligand will always form between both copper centers. This is established by the 1,8-naphthyridine backbone that forces both copper atoms together and avoids catalysis at a single copper site. A first-order dependence in substrate and catalyst for the HPRR and ORR further support this reactivity at a dicopper site. Moreover, the bridged binding of reaction intermediates previously reported by Lippard<sup>36</sup> and observed herein for the  $[\text{Cu}_2\text{L}(\mu\text{-OH})_2]^{2+}$  species, underlie cooperativity between both copper sites during catalysis. In addition, the mechanism of the ORR and HPRR found for  $[\text{Cu}_2\text{L}(\mu\text{-OH})]^{3+}$  differ from the ones found for  $\text{Cu}(\text{tmpa})$ , resulting in improved selectivity for the four-electron ORR of more than 70% as a result of metal-metal cooperativity. Subsequently, we can link the activity and selectivity of this homogeneous catalyst to the ORR mechanism found in MCOs. In both the synthesized  $[\text{Cu}_2\text{L}(\mu\text{-OH})]^{3+}$  complex and T3 site of the MCO resting state a  $\mu$ -OH ligand is present.<sup>12</sup> From our study it is apparent that the formation of the Cu-OH-Cu motif is a severe thermodynamic driving force, hence the presence of the bridging hydroxyl ligand can be linked to slow electron transfer kinetics and a large energy barrier to activate the catalyst. This is comparable to what is observed for MCOs, where the presence of the  $\mu$ -OH makes reduction of the RO state too slow to be part of the catalytic cycle.<sup>20</sup>

In the enzymatic pathway an oxygen molecule can bind to the FR state of MCOs resulting in the formation of a  $\mu_3$ -1,1,2-peroxy intermediate in an irreversible manner.<sup>57</sup>

The binding mode of the  $\mu_3$ -1,1,2 peroxide is essential for the cleavage of the O-O bond and the four-electron reduction of oxygen.<sup>57</sup> When  $[\text{Cu}_2\text{L}]^{2+}$  reacts with oxygen, the peroxy intermediate binds differently, likely as a  $\mu$ -1,2-peroxide, which was observed previously.<sup>36</sup> However, we can explain the greatly improved selectivity towards the overall four-electron ORR by the ability to bind catalytic intermediates in a bridging manner, which is not possible for the mononuclear analogue  $\text{Cu}(\text{tmpa})$ .

To complete the catalytic ORR cycle in MCOs, the second two-electron reduction and cleavage of the O-O bond result in formation of the NI state containing a  $\mu_3$ -O and  $\mu$ -OH.<sup>17</sup> Next, the FR state is regenerated rapidly by protonation and reduction of this highly basic  $\mu_3$ -O ligand.<sup>19</sup> In  $[\text{Cu}_2\text{L}(\mu\text{-OH})]^{3+}$ , a  $\mu_3$ -oxo cannot form, instead we hypothesize that  $[\text{Cu}_2\text{L}(\mu\text{-OH})]^{3+}$  is regenerated upon the two electron reduction of the hydroperoxy intermediate, which is more reminiscent of the decay of NI to RO.

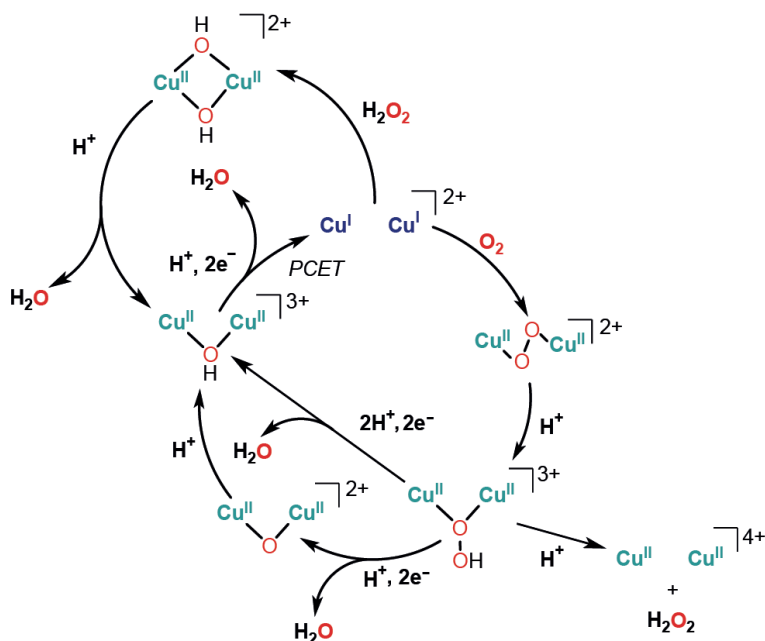


**Figure 4.9** Proposed stepwise mechanism for the ORR and HPRR by  $[\text{Cu}_2\text{L}(\mu\text{-OH})]^{3+}$ . For clarity the BPMAN ligand is not depicted. PCET step takes place below pH 7.

### 4.3 Conclusion

To conclude, by combining electrochemical measurements and reactivity studies, insights into the mechanisms of the ORR and HPRR catalyzed by  $[\text{Cu}_2\text{L}(\mu\text{-OH})]^{3+}$  have been obtained. Some of the key active species along these catalytic pathways were

identified, resulting in a detailed understanding of the activity and selectivity of this catalyst. From our study it is evident that metal-metal cooperativity during both HPRR and ORR could be established by the rigid dinucleating 1,8-naphthyridine-based ligand that keeps both copper atoms in  $[\text{Cu}_2\text{L}(\mu\text{-OH})]^{3+}$  closely together during catalysis. Until now, no other studies on biomimetic copper complexes have given such direct evidence for cooperativity during electrocatalysis of the ORR or HPRR. Following from this, the dinuclear  $[\text{Cu}_2\text{L}(\mu\text{-OH})]^{3+}$  complex catalyzes the HPRR and ORR in a different manner than its mononuclear analogue  $\text{Cu}(\text{tmpa})$ .<sup>35, 51</sup> Due to the presence of the Cu-OH-Cu motif in  $[\text{Cu}_2\text{L}(\mu\text{-OH})]^{3+}$  the dicopper core is stabilized and its reduction follows a PCET pathway. Moreover, the (hydro)peroxo intermediates that can form during the HPRR and ORR are bound between both copper centers, and as a result the formation of hydrogen peroxide is disfavored and the selectivity for the four-electron reduction of oxygen is greatly improved. Taken together, this work helps explain how the electrocatalytic activity and selectivity of the ORR are affected by a rigid dinuclear copper site, which ultimately can be used for the development of oxygen reduction catalysts based on earth abundant metals.

## 4.4 Experimental

### 4.4.1 General

All manipulations were performed under inert atmosphere using standard Schlenk techniques or inside of a  $\text{N}_2$ -filled MBRAUN LABmaster DP glovebox using anhydrous solvents and reagents, unless noted otherwise. Glassware was dried at 130 °C prior to use. Solvents were collected from an MBRAUN MB-SPS-800 solvent purification system and stored over 4 Å molecular sieves, except for  $\text{CH}_2\text{Cl}_2$ , which was stored over 3 Å molecular sieves. Acetonitrile was stored over 3 Å molecular sieves before being passed over a pad of activated alumina. Deuterated solvents were obtained from Cambridge Isotope Laboratories, degassed, and stored over 3 Å molecular sieves when necessary.  $\text{D}_2\text{O}$  for the kinetic isotope experiments was obtained from Eurisotop (99.9 % D). All commercial reagents were used as received and were obtained from Sigma Aldrich, Strem or Acros. All electrolyte solutions were prepared using high purity salts,  $\text{NaH}_2\text{PO}_4$  (Merck, Suprapur  $\geq 99.99$  %),  $\text{Na}_2\text{HPO}_4$  (Honeywell Fluka, TraceSELECT  $\geq 99.999$  %),  $\text{Na}_2\text{SO}_4$  (Alfa Aesar, Puratronic 99.9955 %),  $\text{NaClO}_4 \cdot \text{H}_2\text{O}$  (Merck, EMSURE  $\geq 99.7$  %),  $\text{H}_3\text{BO}_3$  (Sigma-Aldrich, 99.999 % trace metals basis),  $\text{CH}_3\text{COOH}$  (Honeywell Fluka, Trace SELECT  $\geq 99.0$  %),  $\text{H}_3\text{PO}_4$  (85 wt. % in  $\text{H}_2\text{O}$ , Sigma-Aldrich, 99.999% trace metals basis) and Mili-Q water.  $\text{H}_2\text{O}_2$  solution was obtained as a 30 wt% solution in water (Merck) and diluted to the desired concentration. The  $\text{H}_2$ ,  $\text{O}_2$ , and Ar gases used in electrochemical experiments were supplied by Linde.

NMR data was recorded on an Agilent MRF 400 equipped with a OneNMR probe and Optima Tune system or a Varian VNMR-S-400 equipped with an AutoX probe. All resonances in  $^1\text{H}$ -NMR were referenced to residual proteo solvent peaks (7.26 for  $\text{CDCl}_3$ , 7.16 for  $\text{C}_6\text{D}_6$ , 5.32 for  $\text{CD}_2\text{Cl}_2$  and 4.79 for  $\text{D}_2\text{O}$ ). The respective  $^{19}\text{F}$  NMR spectra were referenced employing absolute referencing using the  $^1\text{H}$  NMR spectrum of the same sample. EPR spectra were recorded on a Bruker EMXPlus X-band spectrometer. UV-Vis data was recorded on a PerkinElmer Lambda950 spectrophotometer or an Agilent Varian Cary 50 spectrophotometer. The pH of the electrolyte solutions was altered by addition of diluted solutions of  $\text{NaOH}\cdot\text{H}_2\text{O}$  (Merck, Suprapur 99.9%) or  $\text{H}_2\text{SO}_4$  (96%, Merck, Suprapur). The pH of all electrolyte solutions was determined on a HI 4222 pH meter (Hanna Instruments). The concentration of  $\text{H}_2\text{O}_2$  in aqueous solution was determined with  $\text{H}_2\text{O}_2$  test strips by use of photometric determination with the Merck Reflectoquant system.

#### 4.4.2 Electrochemistry measurements

All electrochemical measurements were recorded using Autolab PGSTAT 12, 204, or 128N potentiostats and Autolab NOVA 2 software. In all stationary CV experiments, except EQCM, the working electrode was a PEEK encapsulated glassy carbon (GC) disk ( $A = 0.071 \text{ cm}^2$ , Metrohm) submerged in the electrolyte solution. This GC electrode was polished prior to every experiment on a Struers LaboPol-30 polishing machine with diamond polish ( $1.0 \mu\text{m}$ , 30 seconds) and silica suspension ( $0.04 \mu\text{m}$ , 2 minutes) on polishing cloths (Dur-type). Afterwards, the GC electrode was sonicated in Mili-Q water for 15 minutes to remove excess polishing solution. In all experiments a gold wire counter electrode was used, which was flame annealed and rinsed with Mili-Q before every experiment. For all measurements in aqueous solutions, a reversible hydrogen electrode (RHE) was used. This RHE was made from a Pt mesh and filled with electrolyte solution.  $\text{H}_2$  was bubbled through the solution during the experiment and the RHE was connected to the main cell compartment via Luggin capillary. Before every electrochemical experiment, the electrolyte solution was bubbled with either Ar or  $\text{O}_2$  gas for at least 15 minutes. During the experiment a flow of the gas was applied over the solution. All electrochemical experiments were carried out in custom-built glass cells that were boiled and rinsed with Mili-Q water prior to every experiment. In addition, the glassware was routinely cleaned by soaking in a solution of  $\text{KMnO}_4$  (1 g/L) in 0.5 M  $\text{H}_2\text{SO}_4$  overnight. Afterwards, the glassware was placed in a diluted solution of  $\text{H}_2\text{SO}_4$  and  $\text{H}_2\text{O}_2$ , rinsed and boiled three times in Mili-Q. Unless stated otherwise, background corrected currents are obtained by subtracting the currents observed in the blank electrolyte solution with no catalyst present under identical conditions, measured directly before measuring the analyte solution.

For pH studies, a 0.01 M Britton-Robinson buffer was prepared by making a solution of 0.01 M  $\text{H}_3\text{BO}_3$ , 0.01 M  $\text{CH}_3\text{COOH}$ , and 0.01 M  $\text{H}_3\text{PO}_4$ . In addition, 0.05 M  $\text{Na}_2\text{SO}_4$  was added as supporting electrolyte. The pH of the solution was changed by addition of

small quantities of 1 M H<sub>2</sub>SO<sub>4</sub> and 1 M NaOH solutions. Between measurements, the solution was vigorously bubbled to ensure proper mixing.

For CV experiments in acetonitrile solution, the glassware was dried in an oven at 140 °C overnight after boiling in MiliQ. The acetonitrile used in electrochemical experiments was either used as received (ACROS, 99.9%, dry) or taken from a PureSolv MD5 solvent dispenser (Demaco) and stored on molecular sieves. Tetrabutylammonium hexafluorophosphate (TBAPF<sub>6</sub>, Sigma-Aldrich, ≥99.0 %) was used to make a 0.1 M electrolyte solution. Triethylammonium hexafluorophosphate (TEAPF<sub>6</sub>) was synthesized from NH<sub>4</sub>PF<sub>6</sub> and triethylamine. Acetic acid was obtained from Sigma-Aldrich (≥99.99 %). Instead of an RHE, Ag/AgCl (3 M KCl) was used as a reference electrode. After the experiments, this Ag/AgCl electrode was referenced to Fc/Fc<sup>+</sup> by recording the ferrocene/ferrocenium redox couple directly in the electrolyte solution.

EQCM experiments were performed in a PEEK electrochemical cell. A gold-coated quartz crystal EQCM electrode (Metrohm, 0.35 cm<sup>2</sup>) was used as WE in combination with the Metrohm EQCM potentiostat module. A gold counter electrode and RHE reference electrode were used in the same manner as described for general CV experiments. All EQCM measurements were conducted on a new EQCM electrode and a blank measurement of the electrode was recorded prior to measurements of the catalyst.

For all R(R)DE experiments a Pine Instruments MSR rotator was used in combination with an Autolab PGSTAT 12 potentiostat. R(R)DE measurements were performed in a 40 mL custom-built three-electrode electrochemical cell, with a Au counter electrode and RHE reference electrode prepared in the same manner as for stationary CV experiments. In the R(R)DE cell the gold counter electrode is separated from the main compartment by a glass frit. A Pine Instruments ChangeDisk RRDE electrode (E6R1PK) was used as working electrode. This electrode consists of a PEEK shroud with a GC disk (A = 0.196 cm<sup>2</sup>) surrounded by a Pt ring. Prior to every experiment, the GC disk and Pt ring were polished separately on a Struers LaboPol-30 polishing machine with diamond polish (1.0 μm, 3 minutes) and silica suspension (0.04 μm, 3 minutes) on polishing cloths (Dur-type). Afterwards, the electrode was sonicated in Mili-Q water for 15 minutes. Before every R(R)DE experiment, the electrolyte solution was bubbled with either Ar or O<sub>2</sub> gas for at least 25 minutes. During the experiment the gas was bubbled through the solution.

## 4.5 References

- (1) Shao, M.; Chang, Q.; Dodelet, J. P.; Chenitz, R., *Chem. Rev.* **2016**, *116* (6), 3594-3657.
- (2) Kulkarni, A.; Siahrostami, S.; Patel, A.; Norskov, J. K., *Chem. Rev.* **2018**, *118* (5), 2302-2312.
- (3) Stephens, I. E. L.; Rossmeisl, J.; Chorkendorff, I., *Science* **2016**, *354* (6318), 1378-1379.
- (4) Gasteiger, H. A.; Kocha, S. S.; Sompalli, B.; Wagner, F. T., *Appl. Catal. B* **2005**, *56* (1-2), 9-35.
- (5) Zaman, S.; Huang, L.; Douka, A. I.; Yang, H.; You, B.; Xia, B. Y., *Angew. Chem. Int. Ed.* **2021**, *60* (33), 17832-17852.
- (6) Solomon, E. I.; Sundaram, U. M.; Machonkin, T. E., *Chem. Rev.* **1996**, *96* (7), 2563-2605.

- (7) Mano, N.; Soukharev, V.; Heller, A., *J. Phys. Chem. B* **2006**, *110* 11180-11187.
- (8) Soukharev, V.; Mano, N.; Heller, A., *J. Am. Chem. Soc.* **2004**, *126*, 8368-8369.
- (9) Thorum, M. S.; Anderson, C. A.; Hatch, J. J.; Campbell, A. S.; Marshall, N. M.; Zimmerman, S. C.; Lu, Y.; Gewirth, A. A., *J. Phys. Chem. Lett.* **2010**, *1* (15), 2251-2254.
- (10) Cole, J. L.; Clark, P. A.; Solomon, E. I., *J. Am. Chem. Soc.* **1990**, *112*, 9534-9548.
- (11) Jones, S. M.; Solomon, E. I., *CMLS* **2015**, *72* (5), 869-883.
- (12) Solomon, E. I.; Heppner, D. E.; Johnston, E. M.; Ginsbach, J. W.; Cirera, J.; Qayyum, M.; Kieber-Emmons, M. T.; Kjaergaard, C. H.; Hadt, R. G.; Tian, L., *Chem. Rev.* **2014**, *114* (7), 3659-3853.
- (13) Solomon, E. I.; Augustine, A. J.; Yoon, J., *Dalton Trans.* **2008**, *30*, 3921-3932.
- (14) den Boer, D.; de Heer, H. C.; Buda, F.; Hetterscheid, D. G. H., *ChemCatChem* **2022**, *15* (1).
- (15) Cole, J. L.; Ballou, D. P.; Solomon, E. I., *J. Am. Chem. Soc.* **1991**, *113* (22), 8544-8546.
- (16) Shin, W.; Sundaram, U. M.; Cole, J. L.; Zhang, H. H.; Hedman, B.; Hodgson, K. O.; Solomon, E. I., *J. Am. Chem. Soc.* **1996**, *118*, 3202-3215.
- (17) Palmer, A. E.; Lee, S. K.; Solomon, E. I., *J. Am. Chem. Soc.* **2001**, *123*, 6591-6599.
- (18) Heppner, D. E.; Kjaergaard, C. H.; Solomon, E. I., *J. Am. Chem. Soc.* **2014**, *136* (51), 17788-17801.
- (19) Heppner, D. E.; Kjaergaard, C. H.; Solomon, E. I., *J. Am. Chem. Soc.* **2013**, *135* (33), 12212-12215.
- (20) Yoon, J.; Liboiron, B. D.; Sarangi, R.; Hodgson, K. O.; Hedman, B.; Solomon, E. I., *PNAS* **2007**, *104* (34), 13609-13614.
- (21) Elwell, C. E.; Gagnon, N. L.; Neisen, B. D.; Dhar, D.; Spaeth, A. D.; Yee, G. M.; Tolman, W. B., *Chem. Rev.* **2017**, *117* (3), 2059-2107.
- (22) Mirica, L. M.; Ottenwaelder, X.; Stack, T. D. P., *Chem. Rev.* **2004**, *104*, 1013-1045.
- (23) Serrano-Plana, J.; Garcia-Bosch, I.; Company, A.; Costas, M., *Acc. Chem. Res.* **2015**, *48* (8), 2397-2406.
- (24) Zhang, W.; Moore, C. E.; Zhang, S., *J. Am. Chem. Soc.* **2022**, *144* (4), 1709-1717.
- (25) Fukuzumi, S.; Tahsini, L.; Lee, Y.-M.; Ohkubo, K.; Nam, W.; Karlin, K. D., *J. Am. Chem. Soc.* **2012**, *134* (16), 7025-7035.
- (26) Mangué, J.; Gondre, C.; Pecaut, J.; Duboc, C.; Menage, S.; Torelli, S., *Chem. Commun.* **2020**, *56* (67), 9636-9639.
- (27) Tahsini, L.; Kotani, H.; Lee, Y. M.; Cho, J.; Nam, W.; Karlin, K. D.; Fukuzumi, S., *Chem. Eur. J.* **2012**, *18* (4), 1084-1093.
- (28) Torelli, S.; Orio, M.; Pecaut, J.; Jamet, H.; Le Pape, L.; Menage, S., *Angew. Chem.* **2010**, *122*, 8425-8428.
- (29) Gomila, A.; Le Poul, N.; Kerbaol, J. M.; Cosquer, N.; Triki, S.; Douziech, B.; Conan, F.; Le Mest, Y., *Dalton Trans.* **2013**, *42* (6), 2238-2253.
- (30) van Dijk, B.; Kinders, R.; Ferber, T. H.; Hofmann, J. P.; Hetterscheid, D. G. H., *ChemElectroChem* **2022**, *9* (3), e202101692.
- (31) Tse, E. C.; Schilter, D.; Gray, D. L.; Rauchfuss, T. B.; Gewirth, A. A., *Inorg. Chem.* **2014**, *53* (16), 8505-8516.
- (32) van Dijk, B.; Hofmann, J. P.; Hetterscheid, D. G. H., *Phys. Chem. Chem. Phys.* **2018**, *20* (29), 19625-19634.
- (33) Smits, N. W. G.; Rademaker, D.; Konovalov, A. I.; Siegler, M. A.; Hetterscheid, D. G. H., *Dalton Trans.* **2022**, *51* (3), 1206-1215.
- (34) Thiyagarajan, N.; Janmanchi, D.; Tsai, Y. F.; Wanna, W. H.; Ramu, R.; Chan, S. I.; Zen, J. M.; Yu, S. S., *Angew. Chem. Int. Ed.* **2018**, *57* (14), 3612-3616.
- (35) Langerman, M.; Hetterscheid, D. G. H., *Angew. Chem. Int. Ed.* **2019**, *58* (37), 12974-12978.
- (36) He, C.; DuBois, J. L.; Hedman, B.; Hodgson, K. O.; Lippard, S. J., *Angew. Chem. Int. Ed.* **2001**, *40* (8), 1484-1487.
- (37) Su, X. J.; Gao, M.; Jiao, L.; Liao, R. Z.; Siegbahn, P. E.; Cheng, J. P.; Zhang, M. T., *Angew. Chem. Int. Ed.* **2015**, *54* (16), 4909-4914.
- (38) Biswas, A.; Das, L. K.; Drew, M. G.; Diaz, C.; Ghosh, A., *Inorg. Chem.* **2012**, *51* (19), 10111-10121.
- (39) Bansal, D.; Gupta, R., *Dalton Trans.* **2017**, *46* (14), 4617-4627.
- (40) Smits, N. W. G.; van Dijk, B.; de Bruin, I.; Groeneveld, S. L. T.; Siegler, M. A.; Hetterscheid, D. G. H., *Inorg. Chem.* **2020**, *59* (22), 16398-16409.
- (41) Chowdhury, S. N.; Biswas, S.; Das, P.; Paul, S.; Biswas, A. N., *Inorg. Chem.* **2020**, *59* (19), 14012-14022.
- (42) Hall, S. B.; Khudaisha, E. A.; Hart, A. L., *Electrochim. Acta* **1999**, *44*, 2455-2462.
- (43) van Stroë-Biezen, S. A. M.; Everaerts, F. M.; Janssen, L. J. J.; Tacken, R. A., *Anal. Chim. Acta* **1993**, *273*, 553-560.
- (44) Lee, K. J.; McCarthy, B. D.; Dempsey, J. L., *Chem. Soc. Rev.* **2019**, *48* (11), 2927-2945.
- (45) Macpherson, J. V., *Phys. Chem. Chem. Phys.* **2015**, *17* (5), 2935-2949.
- (46) Costentin, C., *Chem. Rev.* **2008**, *108* (7), 2145-2179.
- (47) Ghosh, D.; Mukherjee, R., *Inorg. Chem.* **1998**, *37*, 6597-6605.
- (48) Haack, P.; Limberg, C., *Angew. Chem. Int. Ed.* **2014**, *53* (17), 4282-4293.
- (49) Lee, K. J.; Elgrishi, N.; Kandemir, B.; Dempsey, J. L., *Nat. Rev. Chem.* **2017**, *1* (5), 1-14.
- (50) Rountree, E. S.; McCarthy, B. D.; Eisenhart, T. T.; Dempsey, J. L., *Inorg. Chem.* **2014**, *53* (19), 9983-10002.

- (51) Langerman, M.; Hetterscheid, D. G. H., *ChemElectroChem* **2021**, *8* (15), 2783-2791.
- (52) Fukuzumi, S.; Kotani, H.; Lucas, H. R.; Doi, K.; Suenobu, T.; Peterson, R. L.; Karlin, K. D., *J. Am. Chem. Soc.* **2010**, *132* (20), 6874-6875.
- (53) Root, D. E.; Mahroof-Tahir, M.; Karlin, K. D.; Solomon, E. I., *Inorg. Chem.* **1998**, *37*, 4838-4848.
- (54) Mahroof-Tahir, M.; Narasimha Murthy, N.; Karlin, K. D.; Blackburn, N. J.; Shaikh, S. N.; Zubieta, J., *Inorg. Chem.* **1992**, *31*, 3001-3003.
- (55) Itoh, K.; Hayashi, H.; Furutachi, H.; Matsumoto, T.; Nagatomo, S.; Tosha, T.; Terada, S.; Fujinami, S.; Suzuki, M.; Kitagawa, T., *J. Am. Chem. Soc.* **2005**, *127*, 5212-5223.
- (56) Karlin, K. D.; Ghosh, P.; Gultneh, Y.; Jacobson, R. R.; Blackburn, N. J.; Zubieta, J., *J. Am. Chem. Soc.* **1988**, *110* (20), 6769-6780.
- (57) Yoon, J.; Solomon, E. I., *J. Am. Chem. Soc.* **2007**, *129* (43), 13127-13136.